Mechanical Properties of Iron Processed by Severe Plastic Deformation

BING Q. HAN, ENRIQUE J. LAVERNIA, and FARGHALLI A. MOHAMED

In the present study, the mechanical properties of Fe processed *via* severe plastic deformation (equal-channel angular pressing (ECAP)) at room temperature were investigated for the first time. The grain size of annealed Fe, with an initial grain size of about 200 μm, was reduced drastically during ECAP. After eight passes, the grain size reaches 200 to 400 nm, as documented by means of transmission electron microscopy (TEM). The value of microhardness during pressing increases 3 times over that of the starting material after the first pass and increases slightly during subsequent pressing for higher-purity Fe. Examination of the value of microhardness after eight passes as a function of post-ECAP annealing temperature shows a transition from recovery to recrystallization, an observation that resembles the behavior reported for heavily deformed metals and alloys. The tensile and compression behaviors were examined. In tension, a drop in the engineering stress–engineering strain curve beyond maximum load was observed both in the annealed Fe and the ECAP Fe. This drop is related to the neck deformation. The fracture surface, examined by scanning electron microscopy (SEM), shows vein patterns, which is different from the dimples found on the fracture surface of annealed Fe. In compression, an initial strain-hardening region followed by a no-strain-hardening region was observed in the ECAP Fe. The yield strength in tension of the ECAP Fe was observed to be higher than that in compression. The strengthening mechanisms and softening behavior are discussed.

I. INTRODUCTION

THE mechanical behavior of bulk nanostructured Fe with grain sizes of $\leq$100 nm, processed *via* consolidation of milled Fe powders[1–6] or by severe plastic deformation,[7] has been the topic of recent work. Inspection of the literature, however, reveals that most of these studies have been limited to microhardness testing,[1] miniaturized-disk bend tests,[2,3] compression,[8] or tension with a microsample,[5] primarily as a result of the limited availability of bulk nanostructured Fe. Moreover, in many cases, tensile deformation of the bulk nanostructured Fe led to failure in the elastic regime, without any macroscopic ductility, presumably due to the existence of processing defects.[5,8] Therefore, no tensile properties from convincing standard or near-standard tensile tests are available to clarify the deformation mechanisms of nanostructured Fe for grain sizes around 100 nm.

In related studies, Takaki *et al.*[4] and Sakai *et al.*[6] used near-standard tensile samples of ultrafine-grained (UFG) Fe, processed *via* consolidation of milled Fe powders, and reported a high tensile strength of 1.8 GPa in Fe and 1.768 GPa in Fe-1.5 pct O, a low ductility of 3.5 pct in Fe and 0.2 pct in Fe-1.5 pct O, and work softening. These studies involved consolidated pure Fe with grain sizes of about 180 nm[4] and a consolidated UFG Fe–0.2 to 1.5 pct O alloy with grain sizes from 600 to 200 nm.[6] Park *et al.* processed carbon steel (Fe-0.15 pct C-0.25 pct Si-1.1 pct Mn) *via* a technique of equal-channel angular pressing (ECAP) for four passes at 623 K.[9] A tensile strength of 940 MPa was obtained from near-standard tensile testing on specimens with equiaxed ultrafine grains of 200 nm. Similarly, an interstitial-free steel (Fe-0.15 pct Mn-0.049 pct Ti) was processed by an accumulative rolling bond,[10] and a tensile strength of 870 MPa was achieved from near-standard tensile testing on specimens with equiaxed ultrafine grains of 420 nm. Despite these recent studies and the implications of their results, the deformation behavior of UFG steels is not fully understood, partly due to complexities associated with different processing approaches (*e.g.*, milling *vs* ECAP) and partly due to chemical effects: many of the systems studied contain multiple elements.

The preceding information indicates that in order to provide insight into the deformation behavior of Fe in the UFG range, it is necessary that (1) microstructural complications arising from major alloying elements or processing flaws be minimized or eliminated, (2) Fe be tested in the bulk form using standard procedures, (3) grain sizes in the range of 100 to 300 nm be used, (4) Fe be tested in both tension and compression, and (5) the effect on deformation of the purity level of Fe in the UFG range be examined.

In the present investigation, the aforementioned requirements were met by (1) selecting two commercial grades of pure Fe that contained no major alloying elements (with the exception of trace elements), (2) processing Fe *via* severe plastic deformation (ECAP), a technique that is capable of producing bulk ultrafine-structured materials (100 to 300 nm) which are free from porosity and other flaws, and (3) investigating the ECAP of Fe in both tension and compression.

It is the purpose of this article to report and analyze the results that were obtained in the present investigation on bulk Fe processed by the ECAP method.

BING Q. HAN, Senior Research Associate, and FARGHALLI A. MOHAMED, Professor, are with the Department of Chemical Engineering and Materials Science, University of California, Irvine, CA 92697-2575. Contact e-mail: famohame@uci.edu ENRIQUE J. LAVERNIA, Professor, is with the Department of Chemical Engineering and Materials Science, University of California, Davis, CA 95616-5294.

Manuscript submitted February 25, 2002.

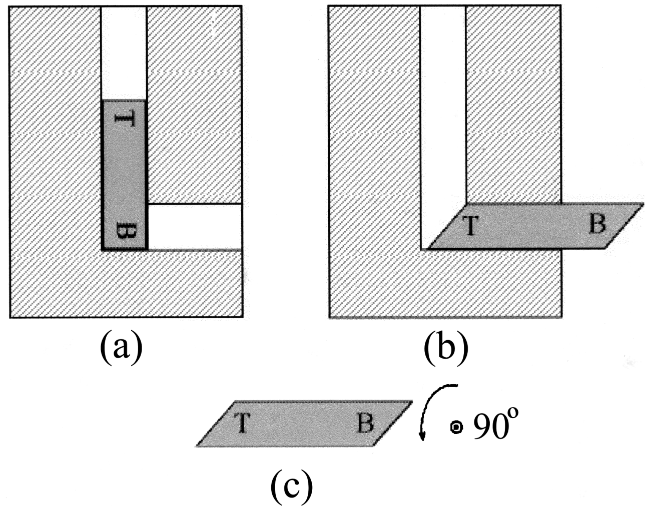

Fig. 1—Schematic illustration of equal-channel angular pressing. Each pass includes three steps: a billet is (*a*) put into the vertical channel, (*b*) pressed into the parallel channel, and (*c*) rotated by 90 deg along its cross section (T: top; and B: bottom).

II. MATERIALS AND EXPERIMENTAL PROCEDURES

The materials used in the present investigation are two commercial grades of Fe, which had different levels of purity and which were received in the form of rods of 9.5 mm in diameter. The 99.95 pct Fe grade (henceforth designated Fe Grade 1) had a composition, in ppm, of Ni 100, O 86, Si 75, Co 34, Al 27, N 11, P 4.8, Ge 4.6, Cr 4.3, Cu 3.9, B 2.8, Ti 1.3, C <1, with the balance as Fe. The 98+ pct Fe grade (henceforth designated Fe Grade 2) had a composition, in ppm (unless otherwise stated), of Mn 0.94 pct, Si 0.31 pct, C 0.2 pct, Cu 1000, Cr 300, Mo 200, Ni 200, Al 100, Co 50, Sn 50, V 30, Ge 10, Ti 3, with the balance as Fe.

The rods were divided into short billets having lengths of ~70 mm, and these billets were subjected to severe plastic deformation using ECAP at room temperature. Before pressing, the annealing treatment of Fe was performed at a temperature of 1203 K for 1 hour in an industrial vacuum furnace. After this treatment, the Fe billets were slowly cooled.

The ECAP die had an internal angle of 90 deg between the two parts of the channel and an outer arc of curvature of ~20 deg where these two parts intersect. It can be shown from first principles that these angles lead to an imposed strain of ~1 on each passage of the sample through the die.[11] In this study, samples were pressed for eight passes for Fe Grade 1 (henceforth designated ECAP-8 Fe), and for one pass for Fe Grade 2 (henceforth designated ECAP-1 Fe). The processing was stopped for the Fe Grade 2 because the ECAP-1 Fe is so strong that the plunger fractured when it was used to press the Fe Grade 2 during the second pressing. During the pressing operation, each sample was rotated by 90 deg in the same direction between consecutive passes through the die, as shown in Figure 1. This procedure is generally termed processing route B_C, and it was selected because it leads most rapidly to a homogeneous microstructure of equiaxed grains separated by high-angle grain boundaries.[12,13]

The cross sections parallel to the processing longitudinal direction were observed by an optical microscope. Transmission electron microscopy (TEM) was performed using a PHILIPS* CM20 microscope operated at 200 kV. The X-ray diffraction (XRD) measurements were carried out along the processing direction with a Siemens D5000 diffractometer (Erlangen, Germany) equipped with a graphite monochromator using Cu K_α radiation ($\lambda = 0.1542$ nm) at 100 steps per deg and a count time of 10 seconds per step. The X-ray tube current and voltage were 30 mA and 40 kV, respectively. The full width at half maximum of the five intense bcc Fe peaks (110, 200, 211, 220, and 310) was measured for annealed Fe Grade 1 and ECAP-8 Fe.

*PHILIPS is a trademark of Philips Electronic Instruments Corp., Mahwah, NJ.

Following each pass, the Vickers microhardness (HV) was measured using a microhardness tester with a diamond pyramidal indenter under a load of 200 g, applied for 15 seconds. The microhardness of ECAP-8 Fe was measured as a function of annealing temperature. Small pieces of samples were annealed in air for 1 hour at various temperatures and mechanically polished prior to microhardness testing. At least seven separate measurements were performed at random sites on the sample surfaces.

Tension and compression testing at ambient temperature was performed using an Instron 8801 universal testing machine (Canton, MA) equipped with a dual-camera video extensometer. The load accuracy is 0.5 pct of the indicated load. The operation of the Instron machine is controlled, and the digital data of load and displacement are recorded, by the Instron Merlin software. The video extensometer allows the measurement of displacement of gage length without mechanical contact with the specimen, through monitoring the movement of gage length. The resolution of the video extensometer is approximately 5 μm. Tensile specimens were tested at a constant crosshead velocity of 0.012 mm/s until failure. The true stress–true strain curve was constructed by using (1) the concept of volume constancy up to the point of maximum load, and (2) the actual cross-sectional area beyond the point of the onset of necking (maximum load). Compression tests were performed at a strain rate of about $10^{-3}\,s^{-1}$, through measuring the displacement of compression platens (including the displacement of specimens and the elastic deformation of platens) by the video extensometer. The elastic deformation of the compression platens, without a sample, was measured after the tests and subtracted from all compression stress-strain curves using a method described in the literature.[14,15]

Tensile and compression specimens were machined from the as-pressed billets with the gage sections lying parallel to the direction of pressing. The materials were sectioned *via* a wire electrodischarge machine into flat pieces along the extrusion direction and were then machined into flat dog bone–shaped specimens, with a gage length of 12 mm, width of 3.6 mm, and thickness of 1.6 mm. In order to understand the effect of heat treatment on the mechanical properties of the ECAP Fe, the material that was annealed for 1 hour at 473 K and cooled in air to ambient temperature was also tested, and the results were compared with those of as-processed Fe. A temperature of 473 K was selected to make sure that the treatment occurs in the recovery region; 473 K is much lower than the recrystallization temperature of

Fe, which depends on the purity of the metal and the amount of prior deformation.

Compression specimens having a cylindrical configuration and a height-to-diameter ratio of 1 were used in the present study. This ratio was chosen on the basis of the results of several preliminary experiments that have shown that ratios less than 1 enhance friction (leading to barreling effect), while ratios more than 1 cause the specimen to buckle.

Tensile specimens for testing at elevated temperatures, with gage lengths of 4 mm, thicknesses of 2 mm, and widths of 3 mm, were used. The tensile experiments at different temperatures were performed using an Instron 1125 testing machine operating with an initial strain rate of 10^{-3} s^{-1}. Each specimen was heated in a furnace to the required testing temperature and then held at this temperature for approximately 30 minutes, in order to achieve thermal equilibrium prior to application of the load. The change of tensile load was recorded as a function of the crosshead displacement using a conventional strip-chart recorder. In the absence of an extensometer for the high-temperature tests, the crosshead displacement was treated as the displacement of the gage length. Samples were pulled to failure to determine a measure of the total elongation under each testing condition.

Scanning electron microscopy (SEM) using a PHILIPS XL30 instrument was used to study the fracture surface of the tensile specimens.

III. EXPERIMENTAL RESULTS

The evolution of microstructure during ECAP of Fe Grade 1 is illustrated in Figure 2. After annealing at 1203 K, the grade has a ferrite grain size of approximately 200 μm, without any apparent preferred orientation (Figure 2(a)).

After pressing for the first pass, the grains are elongated along the pressing direction with an angle of about 27.6 deg, having experienced severe shear deformation (Figure 2(b)). After the second pass, the previous elongated grains are sheared into several shorter segments (Figure 2(c)). After the eighth pass, the grains are sufficiently refined to render them indistinguishable under optical microscopy analysis. The microstructure of ECAP-8 Fe is shown in Figure 3 using TEM. The grain sizes are approximately 200 and 400 nm in the transverse and longitudinal directions, respectively. Moreover, some elongated grains, with dimensions exceeding 600 nm, are also observed. The perfect circular rings in selected-area electron diffraction patterns reveal that the misorientation of the grain boundaries is of a high angle.

The XRD patterns of annealed Fe Grade 1 and ECAP-8 Fe are shown in Figure 4. The figure indicates that as a result of the ECAP process, the intensity of peak (110) in ECAP-8 Fe decreases and that the half-maximum intensity of the diffraction peak is broadened. If the physical origin of peak broadening is attributed to the small size of the diffracting grains only, the volume-averaged grain sizes in the direction perpendicular to the diffraction plane can be determined according to the Scherrer equation:[16]

$$D = 0.9 \cdot \lambda / \Delta(2\theta) \cdot \cos\theta \qquad [1]$$

Where λ is the wavelength of the X-ray radiation, $\Delta(2\theta)$ is the broadening of the diffraction line measured at half-maximum intensity, and θ is the Bragg angle. If the annealed Fe is used as a standard, the actual broadening of the peak is calculated using the following equation: $\Delta(2\theta) = \sqrt{\Delta(2\theta)_2^2 - \Delta(2\theta)_1^2}$, where $\Delta(2\theta)_2$ is the broadening of the diffraction line measured at the half-maximum intensity of

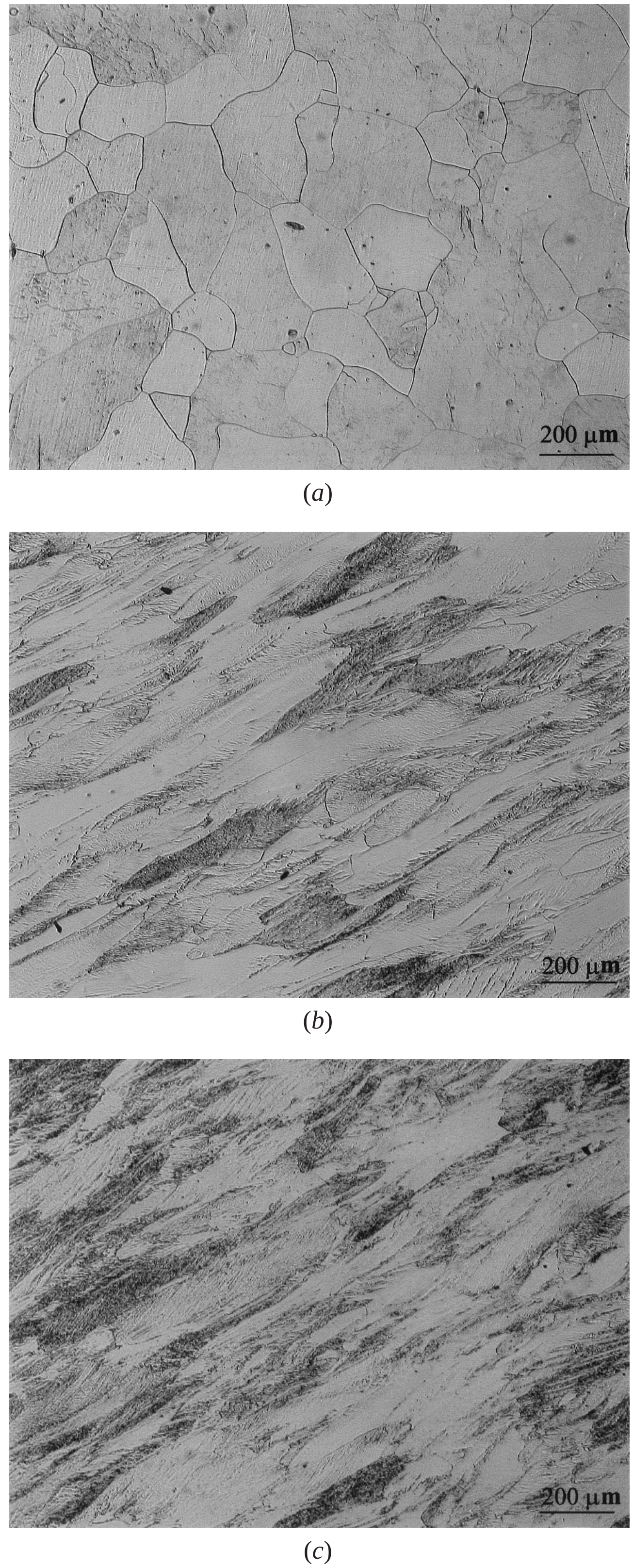

Fig. 2—Microstructure of Fe grade 1 (*a*) after annealing at 1203 K for 1 h before ECAP, (*b*) after the first pass, and (*c*) after the second pass along the longitudinal direction.

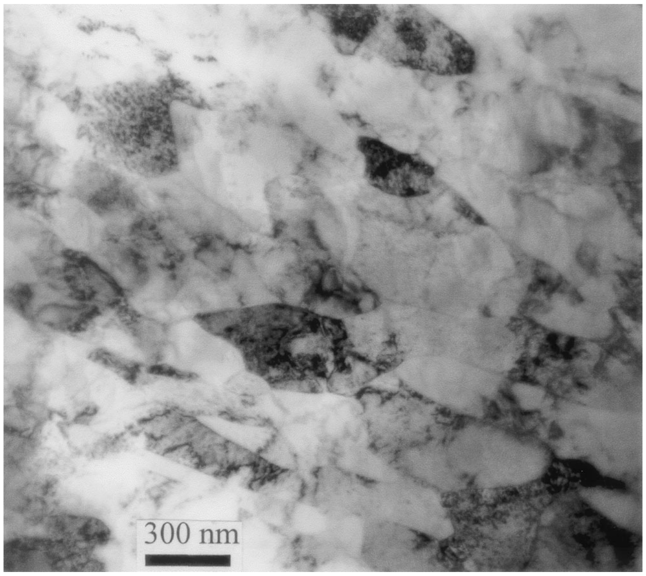

Fig. 3—TEM of Fe grade 1 after eight passes.

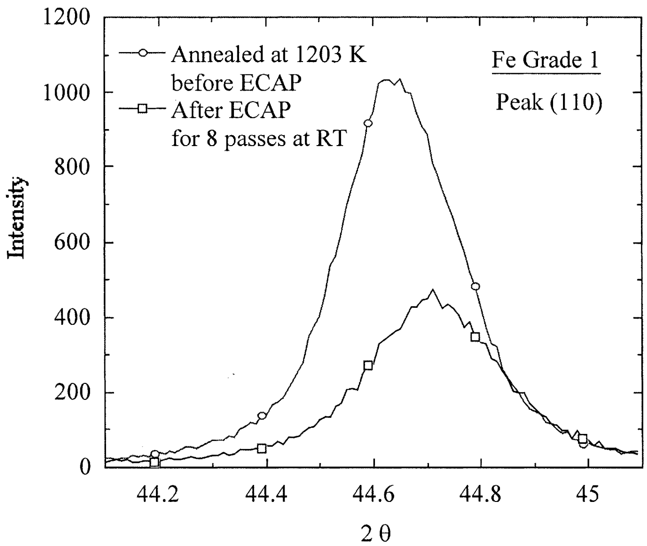

Fig. 4—X-ray diffraction pattern of Fe grade 1.

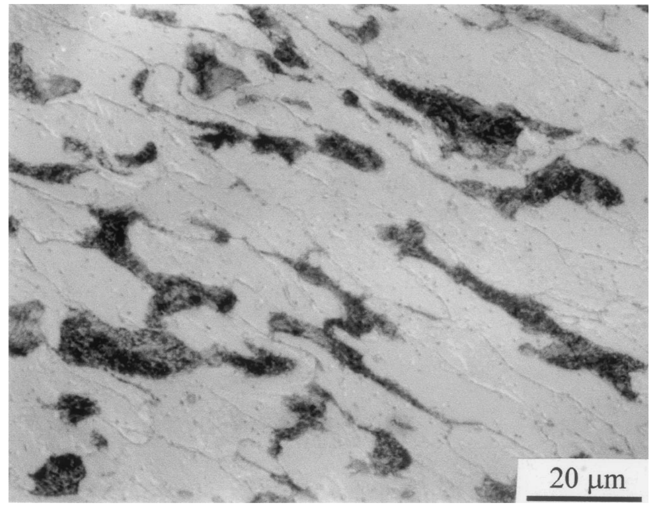

Fig. 5—Microstructure of Fe grade 2 after the first pass.

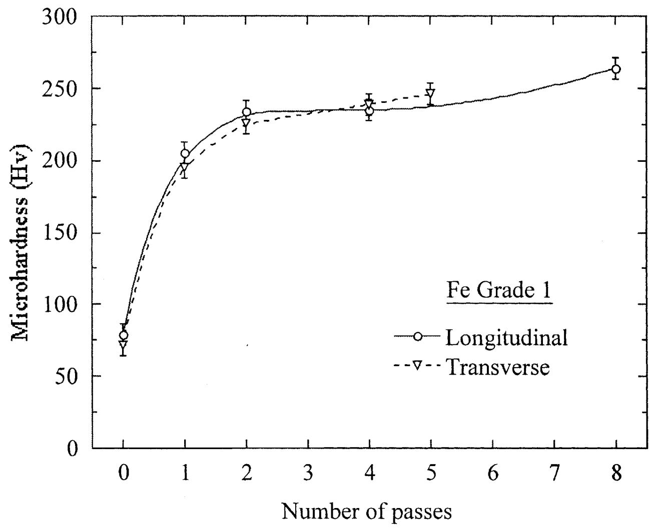

Fig. 6—Evolution of microhardness of Fe grade 1 with the number of pressing.

ECAP-8 Fe, and $\Delta(2\theta)_1$ is the broadening of the diffraction line measured at the half-maximum intensity of annealed Fe. Accordingly, the grain sizes of ECAP-8 Fe are calculated to be about 187 nm using the small-angle, high-intensity (110) peak.

If, however, the physical origin of peak broadening is attributed to both the small size of the diffracting grains and the high internal strain introduced during ECAP, the volume-averaged grain sizes (d) and the lattice microstrain (e) can be estimated, from the five strong Fe peaks (110), (200), (211), (220), and (310), by the following equation:[17]

$$\frac{1}{(\delta s)_o} = d - 4 \cdot e^2 \cdot d \cdot \left(\frac{s}{(\delta s)_o}\right)^2 \qquad [2]$$

where s is the reciprocal space variable ($s = 2 \sin \theta/\lambda$), and $(\delta s)_o$ is the measured peak width. By performing a least-squares fit to $1/(\delta s)_o$ plotted against $(s/(\delta s)_o)^2$ for all the measured peaks of ECAP-8 Fe, d and e are determined to be about 235 nm and 0.046 pct, respectively.

The microstructure of Fe Grade 2 (the lower-purity Fe) after the first pass is shown in Figure 5. It consists of ferrite grains and pearlite at grain boundaries. After one pass, both ferrite and pearlite are elongated along the pressing direction under severe shear deformation.

The evolution of microhardness in Fe Grade 1 with pressing sequence is shown in Figure 6. The standard deviation of the indentation diagonals, based on at least seven separate random measurements, is less than 2. The absolute value of deviation of microhardness is less than 7.5. The value of the microhardness increases significantly after the first pass, modestly after the second pass, and slightly during subsequent pressing. There is no significant difference of microhardness for different orientations. For comparison, the microhardness of Fe Grade 1 is compared with that of Fe and Grade 2 after the first pass, as shown in Figure 7. After one pass, the microhardness value of Fe Grade 2 is about 287, which is much higher than that of Fe Grade 1 (196).

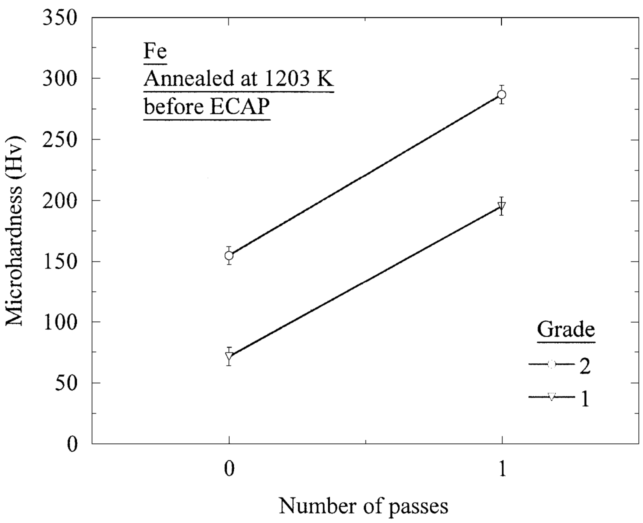

Fig. 7—Comparison of microhardness of Fe grade 1 with Fe grade 2 after the first pass.

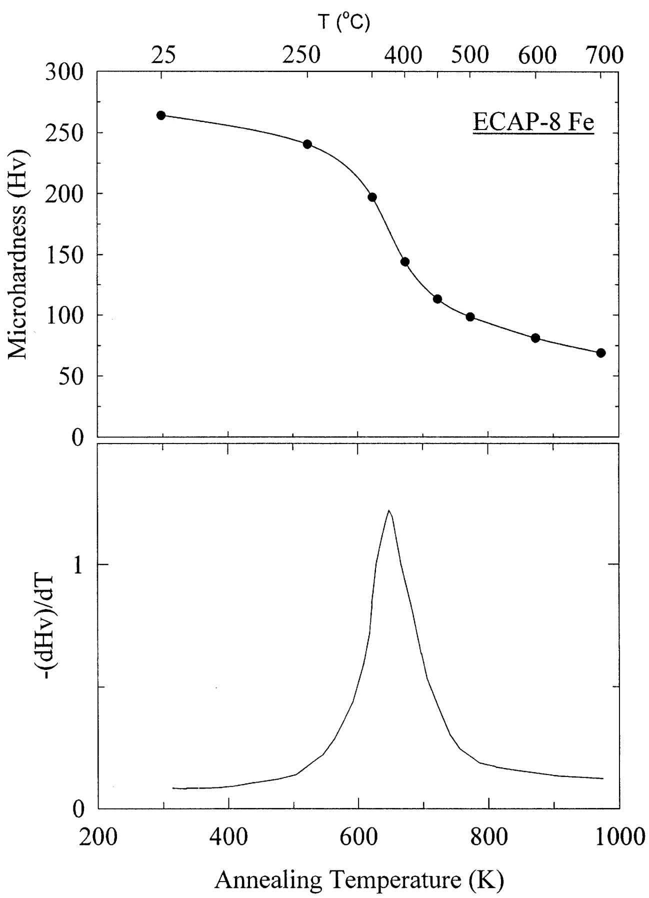

Fig. 8—Evolution of microhardness and the slope of microhardness with annealing temperature of ECAP-8 Fe.

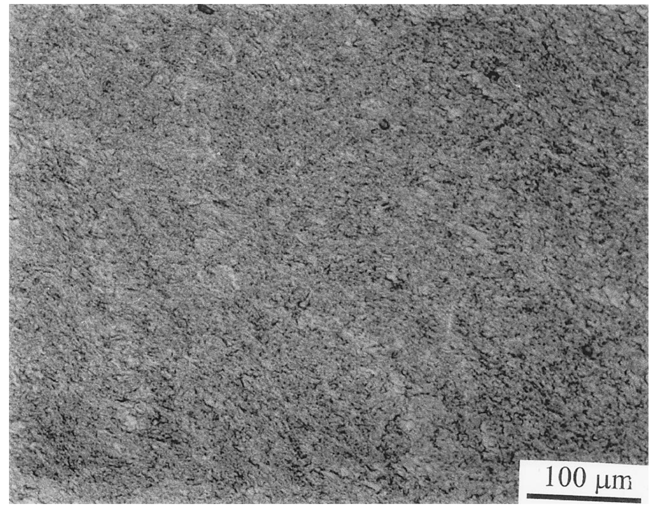

(*a*)

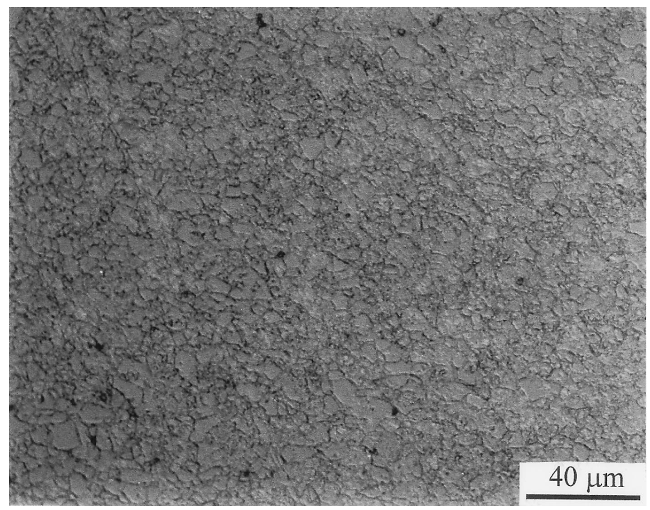

(*b*)

Fig. 9—Microstructure of ECAP-8 Fe for annealing at (*a*) 623 and (*b*) 723 K.

Nevertheless, the increment of microhardness is almost the same after one pass for both materials.

The evolution of microhardness of ECAP-8 Fe after annealing for 1 hour at different temperatures is shown in Figure 8. The values of microhardness decrease with annealing temperature. In order to evaluate the change of microhardness with annealing temperature, the slope ($-d(\mathrm{HV})/dT$) is calculated and also shown in Figure 8. The trend of the slope reveals a transition from recovery to recrystallization. The critical transition temperature (T_{ct}) is approximately 650 K. The microstructure of ECAP-8 Fe after annealing at 623 and 723 K is shown in Figure 9. At the former temperature, because only recovery occurs, there is not much difference in microstructure from that of ECAP-8 Fe. At the latter temperature, because recrystallization is complete, the microstructure consists of newly recrystallized equiaxed grains.

The tensile behavior of the annealed Fe and the ECAP Fe at ambient temperatures, as plotted in the form of engineering stress–engineering strain curves, is shown in Figure 10. The plastic behavior of the ECAP Fe is noticeably different from that of the annealed Fe: the ECAP Fe exhibits a much higher tensile strength than that of the annealed Fe, with a concomitant loss of ductility. After pressing for four passes, the yield strength and the ultimate tensile strength of Fe Grade 1 are approximately 696 and 723 MPa, respectively. There is a short strain-hardening region before continuous geometrical softening sets in. After eight passes, the

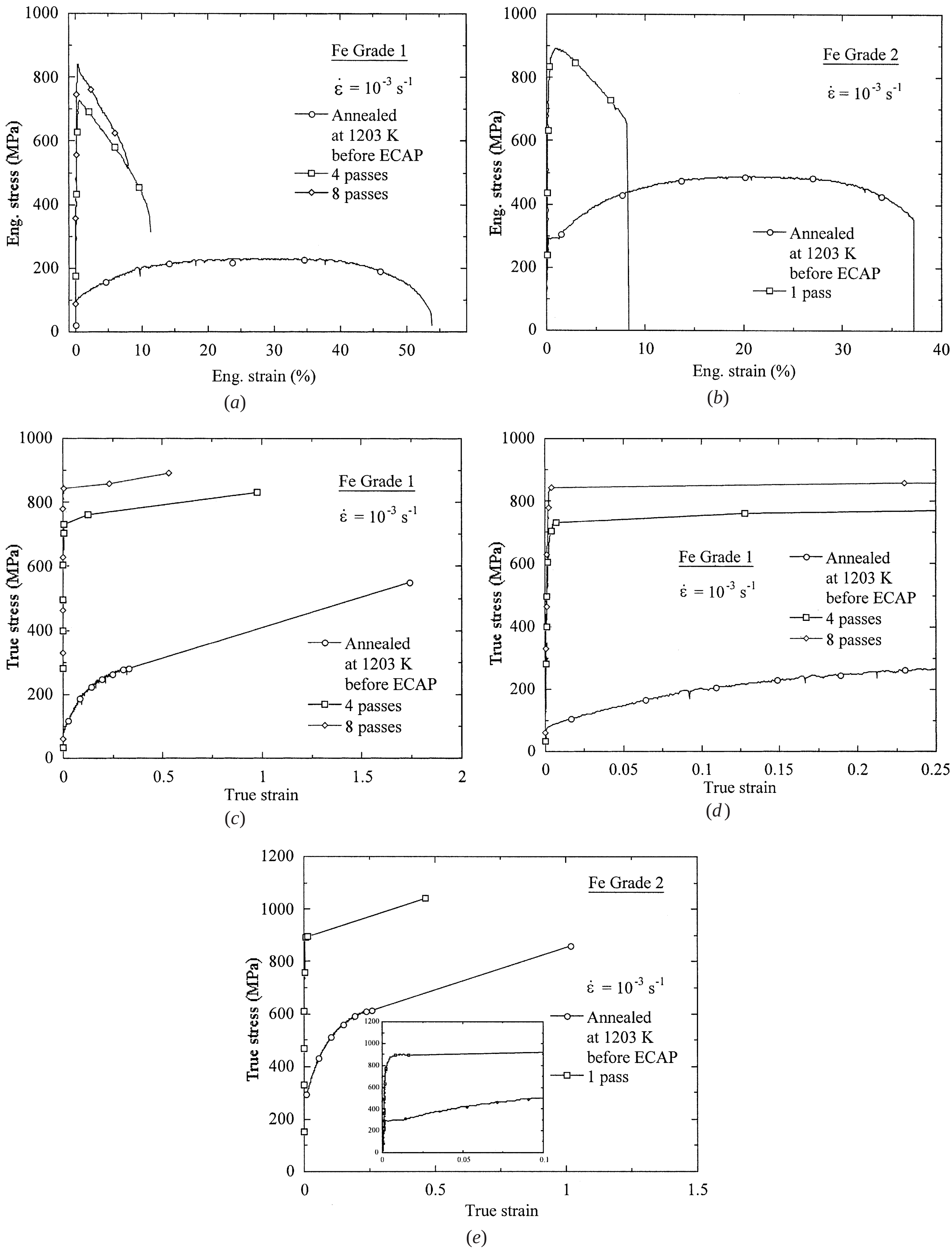

Fig. 10—Tensile properties of Fe (*a*) grade 1 and (*b*) grade 2 in engineering stress-strain curves. Tensile properties of Fe grade 1 (*c*) and (*d*) in true stress-strain curves. Tensile properties of Fe grade 2 (*e*) in true stress-strain curves at ambient temperatures.

ultimate tensile strength increases to 844 MPa. It is worth noting, however, that the ECAP-8 Fe does not exhibit any work hardening following yielding and, moreover, shows a continuous drop in the stress-strain curve and necking immediately at the onset of yielding. Similarly, the ultimate tensile strength of Fe Grade 2 increases to over 890 MPa after one pass. After the yield stress of 857 MPa, the ECAP-1 Fe exhibits a short period of strain hardening and then a continuous drop in the stress-strain curve with the accompanying necking. Serrated flow is observed in the stress-strain curves of both annealed Fe and ECAP Fe.

The true stress–true strain curves for the annealed Fe and the ECAP Fe are plotted in Figures 10(c) through (e). A close examination of these curves indicates that they are similar with respect to the following aspect: a continuous increase in the true stress occurs. In Figure 10(d), the scale is different from that in Figure 10(c), for the purpose of showing the elastic behavior and yielding that cannot be clearly seen in Figure 10(c). This finding indicates that the drop in the value of the engineering stress in Figures 10(a) and (b) reflects geometrical softening due to neck deformation.

It is worth mentioning that an inspection of the neck formed during deformation shows the presence of two primary characteristics: (1) the neck assumes the shape of a narrow band with a width nearly equal to the thickness of the sample, and (2) the neck is inclined at an angle of α to the specimen axis. By measuring this angle from several specimens, it was found that its value was nearly close to 60 deg. These characteristics are consistent with those reported for local necking in a sheet specimen. Also, there is a very small, narrow diffusive neck extending to the two sides of the local neck.

In order to clarify the effect of recovery on strength, the tensile properties of ECAP-4 Fe and ECAP-8 Fe after annealing for 1 hour at 473 K are examined, as shown in Figure 11. There is a minor effect of annealing on the strength of ECAP-4 Fe (Figure 11(a)), but, rather, a significant effect on the strength of ECAP-8 Fe (Figure 11(b)). In specimens with eight passes and subsequent annealing, an extended strain-hardening region appears before reaching the ultimate tensile strength. Moreover, both the yield stress and the ultimate tensile strength are reduced, while ductility is improved.

The plots of engineering stress–engineering strain at elevated temperatures, above and below the critical point T_{ct}, are shown in Figure 12. At a temperature of 623 K, the shapes of the stress-strain curve of ECAP Fe are similar to that at room temperature with regard to the presence of maximum strength and the subsequent occurrence of a continuous drop in the level of stress (Figure 12(a)), because only recovery takes place. At a temperature of 723 K, the shape of the stress-strain curve of ECAP Fe is different from that obtained at room temperature (Figure 12(b)). This difference is manifested by the observation that the peak region at 723 K is broad, because recrystallization takes place.

Fracture surfaces, as shown in Figure 13, are examined by SEM. The fracture surface of annealed Fe Grade 1 (Figure 13 (a)) consists of dimples with slip steps, indicative of intensive plastic deformation. The fracture surface of ECAP-8 Fe (Figures 13(b) and (c)) has vein-like patterns, reminiscent of fracture *via* cleavage, which is different from the

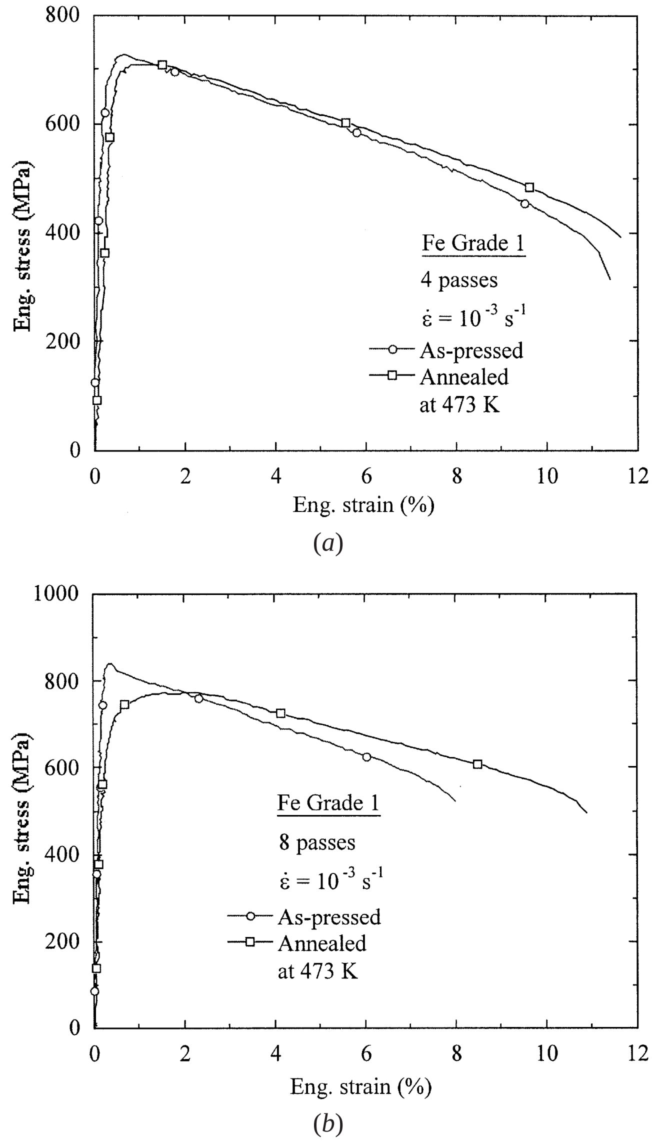

Fig. 11—Tensile properties in engineering stress-strain curves at ambient temperature of (*a*) ECAP-4 and subsequent annealing for 1 h at 473 K and (*b*) ECAP-8 Fe and subsequent annealing for 1 h at 473K.

ductile dimples observed on the fracture surface of annealed Fe and is reminiscent of that of bulk metallic glasses. The fracture surface after tensile testing at room temperature for both annealed Fe Grade 2 and ECAP-1 Fe, as shown in Figures 13(d) and (e), respectively, has a similar shape of dimples, although their plastic deformation is different.

The compression behavior of the annealed and the ECAP Fe at ambient temperatures is compared in Figure 14. As expected, the compressive strength increases significantly after ECAP. Compression of ECAP Fe exhibits perfectly plastic deformation up to high strains without buckling or barreling, whereas there is strain hardening in compression of annealed Fe with uniform deformation. Comparison of the tension and compression behavior in the annealed Fe Grade 1, ECAP-4, and ECAP-8 Fe is shown in Figure 15. It is interesting to note that the compressive yield stress is always lower than the tensile yield stress in the case of the ECAP Fe. The compressive yield stress of annealed Fe is essentially equal to the tensile yield stress, but the strain-hardening exponent in compression is higher than that in

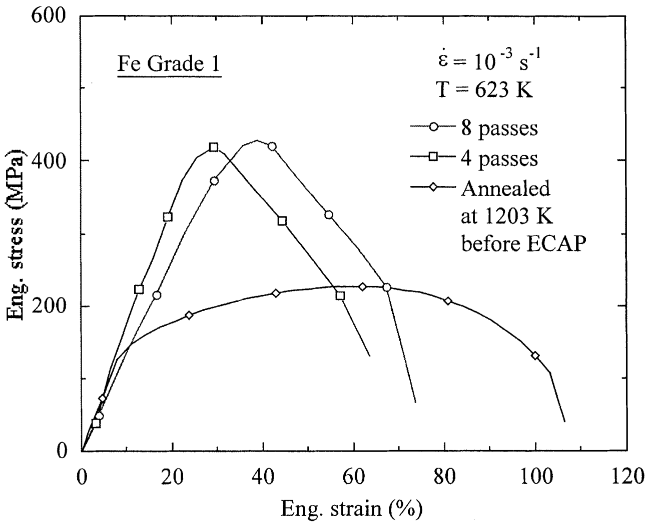

(*a*)

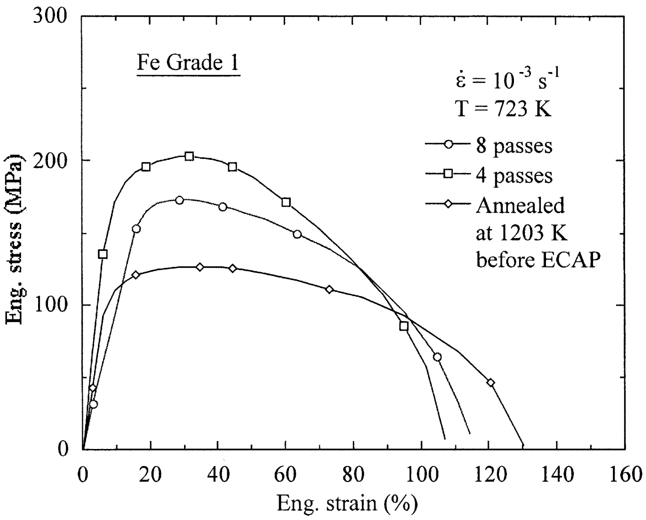

(*b*)

Fig. 12—Tensile behavior in engineering stress-strain curves of Fe grade 1 at elevated temperatures of (*a*) 623 K and (*b*) 723 K.

tension. While the strain-hardening region is either brief or absent in tension for both ECAP-4 and ECAP-8 Fe, noticeable strain hardening after yielding and, subsequently, perfectly plastic deformation are observed in compression. It is interesting to note that serrated flow is observed on the compressive curves of both annealed Fe and ECAP Fe.

IV. DISCUSSION

A. *Thermal Stability of Microstructure of ECAP Fe*

The microstructure of the ECAP Fe, like those of heavily deformed metals, is not thermally stable. The evolution of microhardness with annealing temperature reveals a transition from recovery to recrystallization (Figures 8 and 9). This behavior is also similar to that resulting from the annealing of heavily strained metals. The critical transition temperature of approximately 650 K in ECAP-8 Fe is lower than the recrystallization temperature of electrolytic pure Fe (672 K);[18] the difference between the two temperatures is most likely a reflection of the observation that the recrystallization temperature decreases with increasing amount of prior deformation. This observation is consistent with the finding that the maximum stored energy of the cold-rolled high-purity Fe is released at approximately 673 K, although new grains have clearly formed at 643 K.[19] It is also consistent with the conclusion that metal softening occurs slightly prior to primary recrystallization.[20] Inspection of Figure 8 also indicates that the observed decrease in microhardness due to recovery during annealing is insignificant at temperatures below 523 K, but is significant at temperatures higher than that temperature. The value of microhardness decreases during recovery, as a result of the rearrangement and annihilation of dislocations. It decreases further when recrystallization is nucleated as a result of the release of more stored energy. The process of recrystallization is completed at the critical temperature when the slope ($-d$(HV)/dT) of microhardness with annealing temperature reaches a maximum value. At temperatures higher than the critical temperature, grain growth after recrystallization takes place when the slope decreases with increasing annealing temperature.

It is observed that the subsequent annealing treatment has a minor effect on the plastic deformation of ECAP-4 Fe, but a significant effect on the plastic deformation of ECAP-8 Fe, *i.e.*, an extended strain-hardening region appearing before the softening region along with lower yield and ultimate tensile strengths, as well as better ductility. Although a direct observation on the microstructural evolution of the ECAP Fe *via* TEM is not performed in the present study, the analysis on the microhardness evolution in Figure 6 and the strength difference in Figure 10(a) may provide a possible explanation for this effect. As observed in Figure 6, the value of microhardness rises rapidly after three passes. It is postulated that the density of dislocations introduced by shear deformation increases dramatically and rapidly to a high level after three passes. Moreover, it is possible that dislocations are distributed uniformly in the grains, and grain boundaries (GBs) are mixed up with both low- and high-angle misorientations in the initial deformation. From the third to fourth pass, there is an insignificant increase in microhardness, as a result of a slight increase in the dislocation density. During this period, some of the dislocations around sub-GBs may have been rearranged and annihilated in order to form the GBs with a high-angle misorientation. Nevertheless, GBs are still in an equilibrium structure. During the subsequent severe deformation from four to eight passes, the values of microhardness and strength increase slightly. The high number of accumulated dislocations in the grains are trapped by GBs, causing high internal strain in the vicinity of GBs.[21] Therefore, equilibrium GBs in ECAP-4 Fe are evolved into a nonequilibrium structure in ECAP-8 Fe. The nonequilibrium structure of GBs has an effect on plastic deformation.[21] Moreover, the energy of nonequilibrium GBs can be 2 times higher than that of equilibrium GBs, and, thus, it is unstable, and its relaxation during subsequent annealing leads to the formation of ordered GB dislocation networks.[21] In the present study, subsequent annealing at 473 K may cause an evolution of the GB structure of ECAP-8 Fe from a nonequilibrium structure to an equilibrium one. It should be emphasized that the preceding discussion offers a possible explanation whose

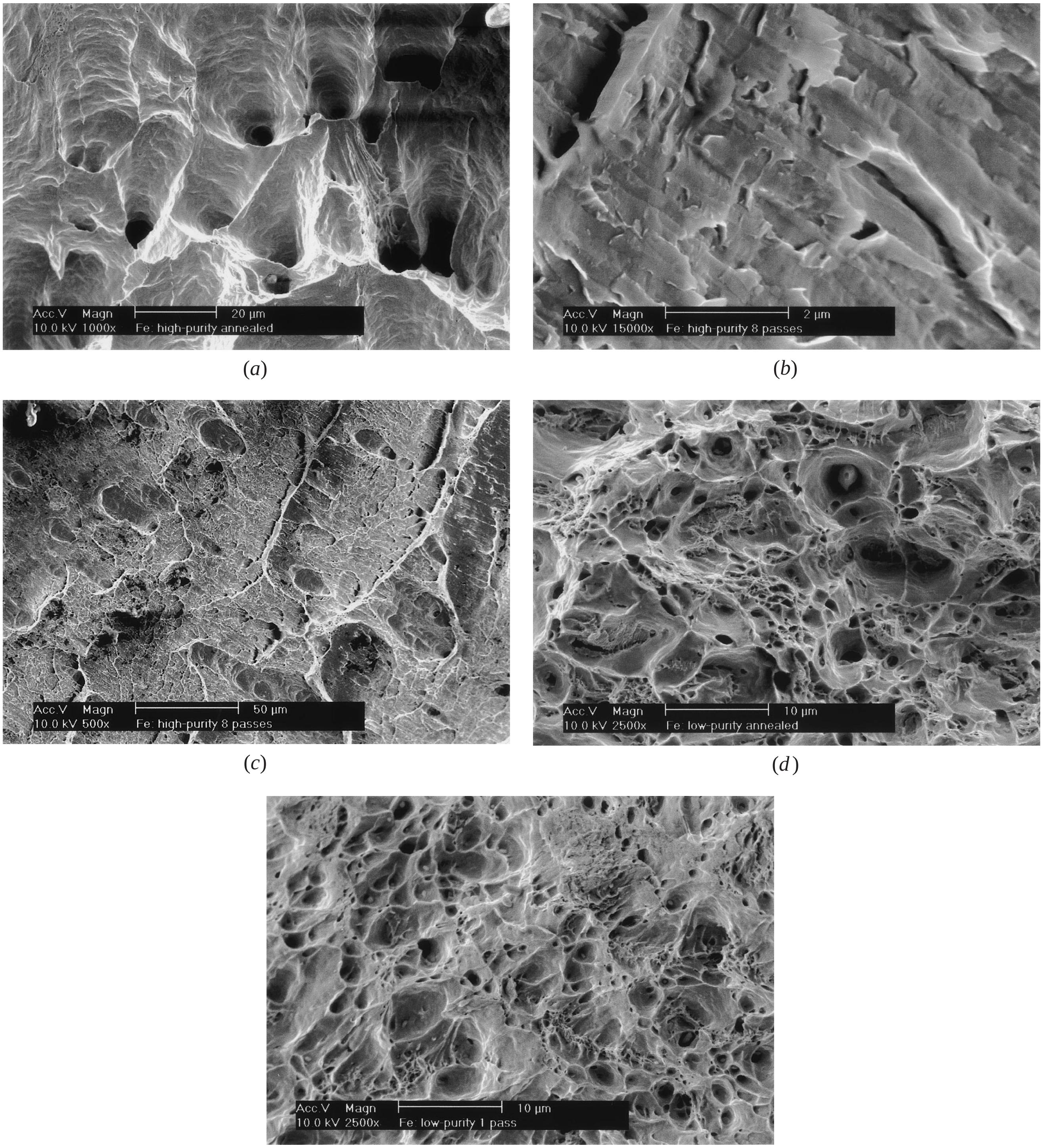

Fig. 13—Fracture surface after tensile testing at room temperature of (*a*) annealed Fe grade 1 and (*b*) and (*c*) ECAP-8 Fe. Fracture surface after tensile testing at room temperature of (*d*) annealed Fe grade 2 and (*e*) ECAP-1 Fe.

validity can be examined in a future investigation focusing on microstructural details in the ECAP Fe.

One comment is in order regarding the characterization of the microstructure. The technique of severe plastic deformation, whether torsion straining under pressure or ECAP, has been used to produce bulk materials that exhibit grain sizes in the range of nanocrystalline structures (1 to 10 nm) to microcrystalline structures (300 nm to 1 mm). The nonequilibrium nature of the microstructure produced and complexity of the boundaries are consistent with the general view held by researchers working in this field (nanostructured materials) that those microstructures are not only metastable, but also complex in nature. In the absence of detailed microstructural investigation, care must be exercised in referring to the microstructure produced *via* severe deformation as a fine-grained structure, in light of early experimental

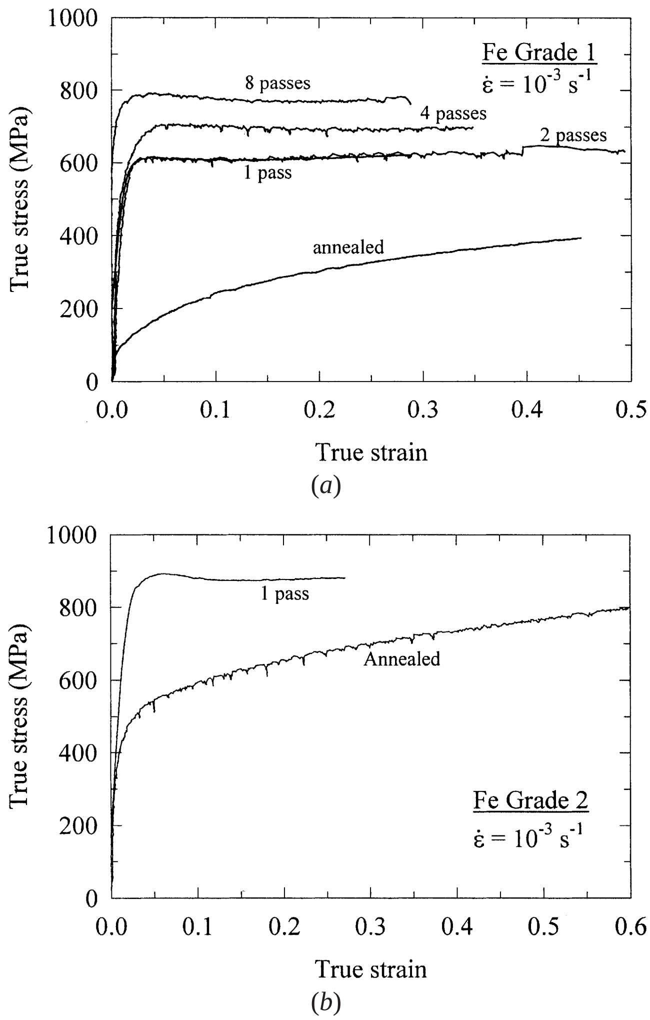

Fig. 14—Compression behavior in true stress-strain curves of (*a*) Fe grade 1 and (*b*) Fe grade 2 at ambient temperatures.

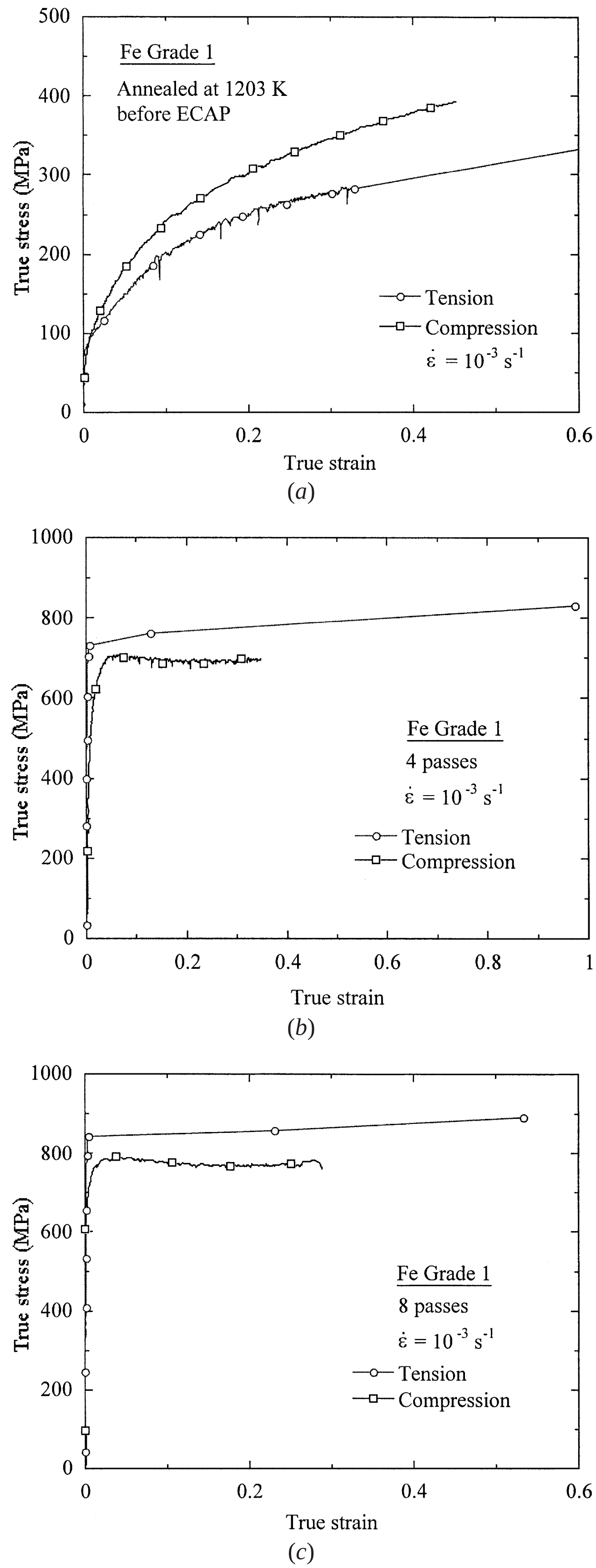

Fig. 15—Comparison of tension and compression behavior in true stress-strain curves of (*a*) annealed Fe grade 1, (*b*) ECAP-4 Fe, and (*c*) ECAP-8 Fe.

evidence. For example, the work of Langford and Cohen on an Fe that was severely deformed *via* drawing indicated that most of the boundaries had less than a 10 deg orientation.[22] There is a difference in deformation between drawing and ECAP: ECAP, unlike drawing, involves severe deformation without a change in the dimensions of the billet. However, despite this difference, the observation reported on the nature of boundaries in the drawn Fe raises a question that is worth addressing whenever some form of severe deformation is applied to a metal.

B. *Strengthening Mechanisms*

The ECAP process can increase hardness and strength significantly, as shown in Figures 6 and 10. After the first and second passes, there is a small change in grain size, but the values of microhardness and strength increase significantly. Obviously, the increment of strength in the first and second passes is not due to the refinement of grains, but can be attributed to the increment of storage of energy in the form of dislocations. Nevertheless, in subsequent pressing, grain sizes have been refined significantly as a result of the rearrangement of high-density dislocations. Segal also

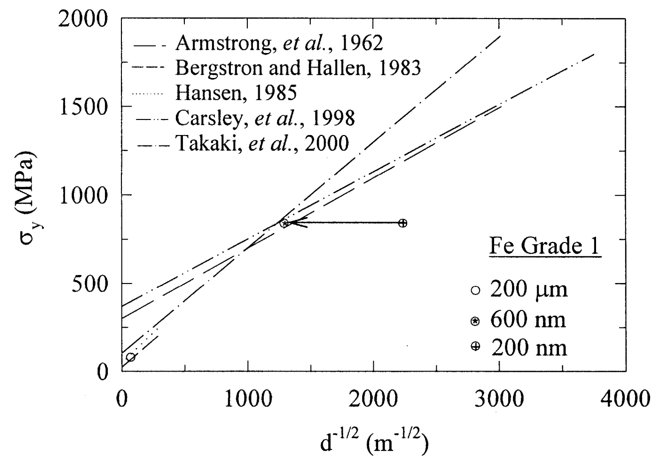

Fig. 16—Grain size effect on yield stress of Fe grade 1.

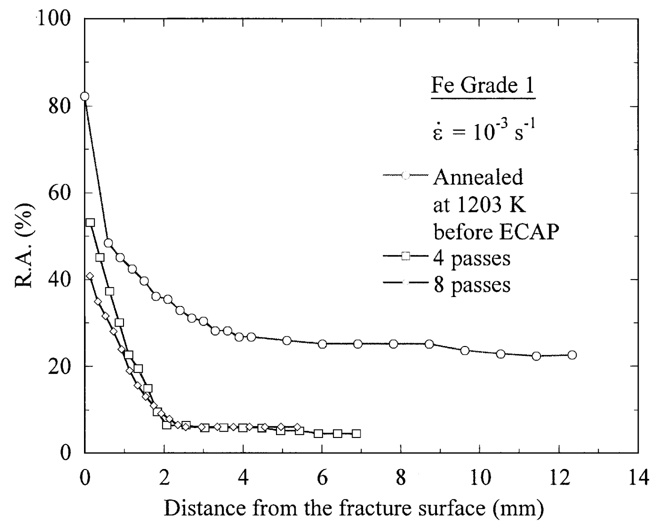

Fig. 17—Reduction of area along the gage length of annealed Fe grade 1, ECAP-4, and ECAP-8 Fe after failure.

reported a similar increase of strength in Armco Fe after the severe plastic deformation of ECAP.[23]

It is well known that the strength increase due to work hardening is expressed by $\Delta\sigma_\perp = M \cdot \alpha \cdot G \cdot b \cdot \rho^{1/2}$, where $M = 2.75$ is the Taylor orientation factor for a bcc structure, and $\alpha = 0.4$ for bcc metals.[24] The density of dislocations of pure Fe by torsion at 293 K was measured to be about $3 \cdot 10^{15}$ m^{-2} at a shear strain of 8.[25] If $G = 64{,}000$ MPa and $b = 2.48 \cdot 10^{-10}$ s^{-1} for α-Fe,[26] and ρ is taken as $3 \cdot 10^{15}$ m^{-2} for ECAP-8 Fe, and $\Delta\sigma_\perp$ is estimated to be 956 MPa. The estimated increment is higher than the actual value of ECAP-8 Fe in the present study. In the present study, the value of $\Delta\sigma_\perp$ between annealed Fe Grade 1 and ECAP-8 Fe is about 761 MPa. Consequently, the increment of actual dislocation densities could be estimated to be about $1.9 \cdot 10^{15}$ m^{-2}. Therefore, it is possible that the density of dislocations in Fe after high-strain deformation is low because of the ease of recovery in pure Fe with a high stacking-fault energy.

From the viewpoint of the grain-size effect, grain refinement is responsible for strengthening *via* the Hall–Petch relationship: $\Delta\sigma_d = k_y \cdot d^{-1/2}$, where k_y is a locking parameter. Inspection of the literature shows that the value of k_y is about 0.6 MN/m$^{3/2}$ for pure Fe; for instance, $k_y = 0.583$ MN/m$^{3/2}$ for Armco Fe,[24] $k_y = 0.6$ MN/m$^{3/2}$ for 99.9 pct Fe[27] and bulk Fe consolidated from milled Fe powders,[4] and $k_y = 0.68$ MN/m$^{3/2}$ for Orkla Fe.[28] The grain-size effect on yield stress is shown in Figure 16. Several data from other nanostructured Fe samples are also shown in the figure. The yield stress of the annealed Fe Grade 1 agrees with the Hall–Petch relationship of pure Fe[27,28] and is slightly lower than that of pure Fe consolidated from milled Fe powders.[4] If the average grain size of ECAP-8 Fe is taken as 200 nm, the corresponding strength is much lower than that of pure Fe, as predicted on the basis of the Hall–Petch relationship. Although the misorientation of grain boundaries has an effect on values of k_y (for instance, there is a lower k_y value in highly strained 0.13 C steel with low-angle GBs[29]), the lower yield stress of pure Fe at grain sizes of 200 nm cannot be attributed to low-angle GBs. Alternatively, it may be argued that the reason for this discrepancy is that the flow stress may be influenced by the presence in the microstructure of elongated grains, with dimensions exceeding 600 nm (Figure 3). If deformation is initiated in some of these elongated, large grains under the action of the applied stress, it is quite possible that the occurrence of such deformation produces stress concentrations that spread yielding into smaller grains.

C. *Plastic Deformation*

The neck deformation is one of the primary differences in plastic deformation between the annealed Fe and the ECAP Fe. The reduction of area along the gage length of annealed Fe Grade 1, ECAP-4, and ECAP-8 Fe after tensile failure is shown in Figure 17. The values of reduction of area at the point of the fracture in the present study for pure Fe are smaller than those of some carbon steels.[29] While the deformation in the annealed Fe is relatively uniform, the deformation in the ECAP Fe is heterogeneous, and most of the deformation is restricted to the vicinity of the necking region. It is noted that the plastic deformation of the ECAP Fe is localized and restricted to the region of the gage length where the neck is formed. Out of the localized deformed zone, the measurable uniform deformation is very low. As a result of this localized deformation, the total elongation of ECAP-8 Fe is low, only 8 pct, as compared with 43 pct in the annealed Fe Grade 1.

The flow characterizations of the ECAP Fe are different from those of coarse-grained Fe. For the annealed Fe grade 1, after an extended work-hardening region, the ultimate tensile strength is obtained when the necking deformation starts. During the neck deformation, softening takes place. For ECAP-1 Fe, there is a brief work-hardening region following by an extended geometrical softening region. For ECAP-4 Fe, there is a brief work-hardening region following by an extended geometrical softening region. Finally, for ECAP-8 Fe, there is no work-hardening region, but an extended geometrical softening region. The necking deformation is observed in all cases of the ECAP Fe. Even though the rate of geometrical softening in the annealed Fe is slightly faster than that in the ECAP Fe, geometrical softening in the ECAP Fe seems to be related to the necking deformation.

Although the vein-like patterns of the tensile fracture surface in the Fe ECAP observed in the present study are similar to the step-like morphology of a tensile fracture surface in a metallic glass tested at elevated temperatures,[30] tensile deformation of the ECAP Fe is different from that of amorphous glasses in two aspects. First, compared to the plastic strain of about 8 pct observed here in ECAP-8 Fe, there is no measurable plastic deformation in tension at ambient temperatures in metallic glasses. For instance, Cu-Hf-Ti bulk glassy alloys[31] or $Pd_{40}Ni_{40}P_{20}$ bulk metallic glasses[32] failed in the elastic region or right after yielding, and inhomogeneous tensile deformation in the form of shear bands, a kind of plastic instability, is observed. Second, compared to the severe necking deformation in the ECAP Fe, there is no necking deformation at ambient temperatures in metallic glasses.[31,32]

In terms of compressive behavior, the elastic–perfectly plastic deformation reported here for the ECAP Fe is also observed in nanostructured Fe with grain sizes of 80 nm[8] and nanostructured Fe-10Cu,[33,34] as well as metallic glasses.[31] While shear bands were observed to be a dominant deformation mode in nanostructured Fe[8,34] and the only deformation mode in bulk metallic glasses,[31] uniform compression without buckling or barreling in the ECAP Fe is observed at the present study.

In summary, the deformation behavior of the ECAP Fe is different from that of the nanostructured Fe or metallic glasses. It is argued that softening of the ECAP Fe in tension is accompanied by plastic instability (necking). According to Considère's criterion,[24] necking starts at the maximum stress when the increase in strength of the materials due to work hardening is less than the decrease in the load-bearing ability due to the decrease in cross-sectional area. The annealed Fe, with a capacity for strain hardening, would be mechanically stable initially, until the rate of work hardening was equal to the maximum stress. The formation of necking results in an accelerated and localized decrease in the cross-sectional area. The ECAP Fe would become unstable soon after the onset of plastic strain.

As mentioned in Section III, the compressive yield stress of the annealed Fe is essentially equal to the tensile yield stress, but the compressive yield stress is always lower than the tensile yield stress in the case of the ECAP Fe. An inspection of Figure 6 (The XRD patterns) indicates the presence of an apparent peak shift in addition to its broadening. This peak shift to a higher Bragg angle signifies a smaller lattice parameter, which may result from the presence of residual net and large compressive stresses. This possibility may provide an explanation for the lower yield strength in compression.

Serrated flow is observed in both annealed Fe and ECAP Fe when tested in tension and compression. The serrated flow in Fe and steel has been studied extensively and is referred to as dynamic strain aging (the Portevin–Le Chatelier effect), in which the moving dislocations interact with substitutional or interstitial elements.[35,36] In tension and compression of the annealed Fe, the multiplication of dislocations plays a dominant role, and work hardening is revealed.

V. CONCLUSIONS

1. Annealed pure Fe with an initial grain size of approximately 200 μm was processed *via* severe plastic deformation (ECAP) at room temperature. A grain size of approximately 200 nm is obtained after eight passes.
2. The value of microhardness of Fe Grade 1 during the pressing sequence increases 3 times after the first pass and increases slightly during subsequent pressing. The value of microhardness in ECAP-8 Fe decreases with annealing temperature, showing a transition from recovery to recrystallization.
3. In tension, plastic deformation with geometrical softening was observed in the ECAP Fe, which is different from strain hardening in the annealed Fe. The ECAP-8 Fe still has a relatively high elongation of about 8 pct. The fracture surfaces show vein-like patterns, which are different from the dimples on the fracture surfaces of the annealed Fe. In compression of the ECAP Fe, a strain-hardening region followed by perfectly plastic deformation was observed.
4. Dislocation strengthening and a grain-size effect are considered to play a significant role in strengthening of the ECAP Fe.

ACKNOWLEDGMENTS

The work is supported by the Army Research Office under Grant No. DAAD19-01-1-0627. We are thankful to the Review Committee for providing useful suggestions and constructive comments. The ECAP material used in the present investigation was processed at the University of Southern California by one of us (BH), who wishes to express his appreciation to Professor T.G. Langdon.

REFERENCES

1. G.E. Fougere, J.R. Weertman, and R.W. Siegel: *NanoStruct. Mater.*, 1995, vol. 5, pp. 127-34.
2. T.R. Malow and C.C. Koch: *Metall. Mater. Trans. A*, 1998, vol. 29A, pp. 2285-95.
3. T.R. Malow and C.C. Koch: *Acta Mater.*, 1998, vol. 46, pp. 6459-73.
4. S. Takaki, K. Kawasaki, and Y. Kimura: in *Ultrafine Grained Materials*, R.S. Mishra, S.L. Semiatin, C. Suryanarayana, N.N. Thadhani, and T.C. Lowe, eds., TMS, Warrendale, PA, 2000, pp. 247-55.
5. D. Jia, K.T. Ramesh, and E. Ma: in *Ultrafine Grained Materials*, R.S. Mishra, S.L. Semiatin, C. Suryanarayana, N.N. Thadhani, and T.C. Lowe, eds., TMS, Warrendale, PA, 2000, pp. 309-18.
6. Y. Sakai, M. Ohtaguchi, Y. Kimura, and K. Tsuzaki: in *Ultrafine Grained Materials*, R.S. Mishra, S.L. Semiatin, C. Suryanarayana, N.N. Thadhani, and T.C. Lowe, eds., TMS, Warrendale, PA, 2000, pp. 361-70.
7. R.Z. Valiev, Y.V. Ivanisenko, E.F. Rauch, and B. Baudelet: *Acta Mater.*, 1996, vol. 44, pp. 4705-12.
8. D. Jia, K.T. Ramesh, and E. Ma: *Scripta Mater.*, 2000, vol. 42, pp. 73-78.
9. K.T. Park, Y.S. Kim, J.G. Lee, and D.H. Shin: *Mater. Sci. Eng.*, 2000, vol. A293, pp. 165-72.
10. N. Tsuji, Y. Saito, H. Utsunomiya, and S. Tanigawa: *Scripta Mater.*, 1999, vol. 40, pp. 795-800.
11. K. Nakashima, Z. Horita, M. Nemoto, and T.G. Langdon: *Acta Mater.*, 1998, vol. 46, pp. 1589-99.
12. M. Furukawa, Y. Iwahashi, Z. Horita, M. Nemoto, and T.G. Langdon: *Mater. Sci. Eng.*, 1998, vol. A257, pp. 328-32.
13. K. Oh-ishi, Z. Horita, M. Furukawa, M. Nemoto, and T.G. Langdon: *Metall. Mater. Trans. A*, 1998, vol. 29A, pp. 2011-13.
14. M.A. Meyers and K.K. Chawla: *Mechanical Metallurgy Principles and Applications*, Prentice-Hall, Englewood Cliffs, NJ, 1984.
15. B.Q. Han and D.C. Dunand: *Mater. Sci. Eng.*, 2000, vol. A277, pp. 297-304.
16. B.D. Cullity: *Elements of X-ray Diffraction*, Addison-Wesley Publishing Co., Inc., Reading, MA, 1978.
17. H.P. Klug and L. Alexander: *X-ray Diffraction Procedures for Poly-*

crystalline and Amorphous Materials, 2nd ed., John Wiley & Sons, New York, NY, 1974, p. 661.
18. A.K. Sinha: *Ferrous Physical Metallurgy*, Butterworth and Co., London, 1989, p. 98.
19. F. Scholz, J.H. Driver, and E. Woldt: *Scripta Mater.*, 1999, vol. 40, pp. 949-54.
20. P. Cotterill and P.R. Mould: *Recrystallization and Grain Growth in Metals*, Surrey University Press, London, 1976, p. 55.
21. A.A. Nazarov, A.E. Romanov, and R.Z. Valiev: *Acta Metall. Mater.*, 1993, vol. 41, pp. 1033-40.
22. G. Langford and M. Cohen: *Trans. ASM*, 1969, vol. 62, pp. 623-38.
23. V.M. Segal: *Mater. Sci. Eng.*, 1995, vol. A197, pp. 157-64.
24. T.H. Courtney: *Mechanical Behavior of Materials*, 2nd ed., McGraw-Hill Higher Education, New York, NY, 2000.
25. E. Schafler, M. Zehetbauer, A. Borbely, and T. Ungar: *Mater. Sci. Eng.*, 1997, vols. A234–A236, pp. 445-48.
26. H.J. Frost and M.F. Ashby: *Deformation-Mechanism Maps: The Plasticity and Creep of Metals and Ceramics*, Pergamon Press, New York, NY, 1982, p. 32.
27. N. Hansen: *Metall. Trans. A*, 1985, vol. 16A, pp. 2167-90.
28. Y. Bergstrom and H. Hallen: *Met. Sci.*, 1983, vol. 17, pp. 341-47.
29. W.B. Morrison and R.L. Miller: in *Ultrafine-Grain Metals*, J.J. Burke and J. Weiss, eds., Syracuse University Press, Syracuse, NY, 1970, pp. 182-211.
30. T.G. Nieh, J. Wadsworth, C.T. Liu, G.E. Ice, and K.S. Chung: *Mater. Trans.*, 2001, vol. 42, pp. 613-18.
31. A. Inoue, W. Zhang, T. Zhang, and K. Kurosaka: *J. Mater. Res.*, 2001, vol. 16, pp. 2836-44.
32. T. Mukai, T.G. Nieh, Y. Kawamura, A. Inoue, and K. Higashi: *Scripta Mater.*, 2002, vol. 46, pp. 43-47.
33. J.E. Carsley, W.W. Milligan, S.A. Hackey, and E.C. Aifantis: *Metall. Mater. Trans. A*, 1995, vol. 26A, pp. 2479-81.
34. J.E. Carsley, A. Fisher, W.W. Milligan, and E.C. Aifantis: *Metall. Mater. Trans. A*, 1998, vol. 29A, pp. 2261-71.
35. S. Kinoshita, P.J. Wray, and G.T. Horne: *Trans. TMS-AIME*, 1965, vol. 233, pp. 1902-04.
36. B.J. Brindley and J.T. Barnby: *Acta Metall.*, 1966, vol. 14, pp. 1765-80.